CellPress

Neuron
Article

# TMIE Is an Essential Component of the Mechanotransduction Machinery of Cochlear Hair Cells

Bo Zhao,[1] Zizhen Wu,[1] Nicolas Grillet,[1,2] Linxuan Yan,[1] Wei Xiong,[1] Sarah Harkins-Perry,[1] and Ulrich Müller[1,*]
[1]Dorris Neuroscience Center, Department of Molecular and Cellular Neuroscience, The Scripps Research Institute, 10550 N. Torrey Pines Road, La Jolla, CA 92037, USA
[2]Present address: Department of Otolaryngology, Stanford University, 300 Pasteur Drive, Stanford, CA 94305, USA
*Correspondence: umueller@scripps.edu
http://dx.doi.org/10.1016/j.neuron.2014.10.041

## SUMMARY

**Hair cells are the mechanosensory cells of the inner ear. Mechanotransduction channels in hair cells are gated by tip links. The molecules that connect tip links to transduction channels are not known. Here we show that the transmembrane protein TMIE forms a ternary complex with the tip-link component PCDH15 and its binding partner TMHS/LHFPL5. Alternative splicing of the PCDH15 cytoplasmic domain regulates formation of this ternary complex. Transducer currents are abolished by a homozygous *Tmie*-null mutation, and subtle *Tmie* mutations that disrupt interactions between TMIE and tip links affect transduction, suggesting that TMIE is an essential component of the hair cell's mechanotransduction machinery that functionally couples the tip link to the transduction channel. The multisubunit composition of the transduction complex and the regulation of complex assembly by alternative splicing is likely critical for regulating channel properties in different hair cells and along the cochlea's tonotopic axis.**

## INTRODUCTION

Mechanoelectrical transduction, the conversion of mechanical force into electrical signals, is critical for our senses of hearing, balance, proprioception, and touch. In the inner ear, mechanotransduction channels are localized in hair bundles that crown the apical surface of each hair cell. Hair bundles consist of stereocilia that are organized in rows of decreasing heights like the pipes of an organ (Richardson et al., 2011; Schwander et al., 2010). Fine extracellular filaments, the tip links, connect the stereocilia in the direction of the mechanical sensitivity of the hair bundles and are thought to transmit force onto transduction channels (Figure 1A) (Assad et al., 1991; Pickles et al., 1991). Deflections of the hair bundle in the direction of the longest stereocilia lead to increases in the open probability of transduction channels, while deflections in the opposite direction decrease channel open probability (Gillespie and Müller, 2009).

Several components of the mechanotransduction machinery of hair cells have been identified. Genes that are linked to Usher syndrome type 1 (USH1; deaf-blindness) encode many of these components. Tip links are formed by the USH1 proteins CDH23 and PCDH15, which interact to form the upper and lower parts of tip links, respectively (Ahmed et al., 2006; Kazmierczak et al., 2007; Siemens et al., 2004; Söllner et al., 2004). The USH1 proteins harmonin, SANS, and myosin 7a bind to the CDH23 cytoplasmic domain (Adato et al., 2005; Bahloul et al., 2010; Boëda et al., 2002; Siemens et al., 2002), and they colocalize at the upper tip-link density (UTLD) (Grati and Kachar, 2011; Grillet et al., 2009). Harmonin regulates transducer channel activation and adaptation (Grillet et al., 2009; Michalski et al., 2009), and SANS has been proposed to regulate tip-link assembly and mechanotransduction (Caberlotto et al., 2011), indicating that these USH1 proteins form a protein complex at the UTLD that is important to regulate transduction. Myosin 7a might also be important for transduction, although this requires further study (Kros et al., 2002; Marcotti et al., 2014).

The genes that encode the pore-forming subunits of the mechanotransduction channels are currently not well defined. $Ca^{2+}$ enters stereocilia upon mechanical stimulation near the lower tip-link insertion site, indicating that transduction channels are present in proximity to PCDH15 (Beurg et al., 2009). *TMC1*, a gene that is linked to inherited forms of deafness (Kurima et al., 2002), and *TMC2*, a close homolog of TMC1, have been proposed to encode subunits of the mechanotransduction channel (Kawashima et al., 2011; Kim and Fettiplace, 2013), possibly forming its pore (Pan et al., 2013). However, endogenous TMC1 or TMC2 proteins have so far not been detected in stereocilia (Kawashima et al., 2011; Pan et al., 2013), and transducer currents can still be evoked in TMC1/2 mutant mice by deflection of hair bundles in the opposite from normal direction (Kim et al., 2013). Reverse-polarity transducer currents are also observed when tip links are broken (Alagramam et al., 2011; Kim et al., 2013; Marcotti et al., 2014). It has therefore been proposed that TMC1/2 might be accessory subunits of the transduction channel that regulate channel localization to tip links and/or form an extracellular vestibule that controls ion flow toward the channel pore (Marzban et al., 2003; Smalla et al., 2000).

TMHS/LHFPL5 (referred to as LHFPL5 in the following) is an additional protein that is implicated in the regulation of

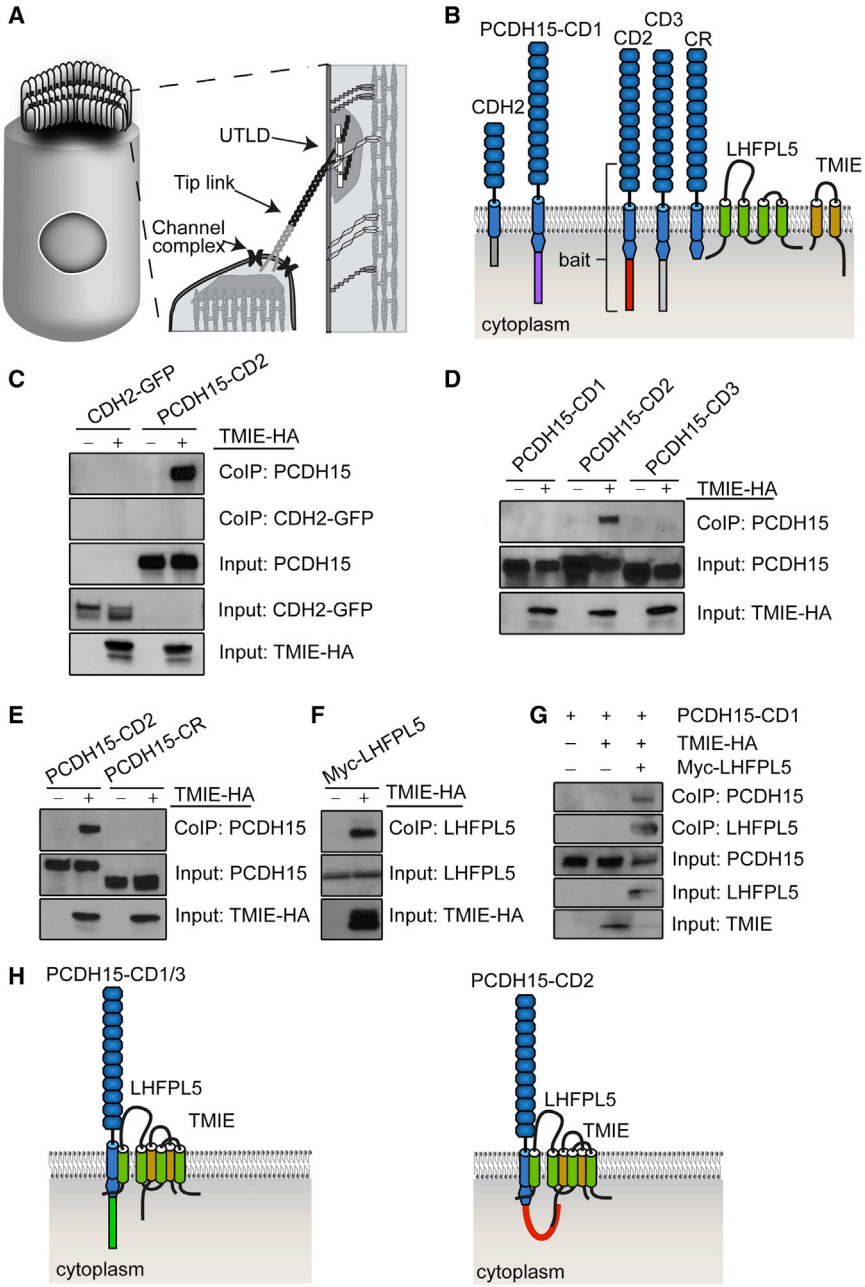


**Figure 1. Interactions of TMIE with PCDH15 and LHFPL5**

(A) Hair cell diagram showing on the right a higher-magnification view of the tip-link region. The upper tip-link density (UTLD), the tip link, and the transduction channel complex are indicated.

(B) Diagram of the constructs used for biochemical experiments. The PCDH15-CD2 domain that was used as bait for yeast two-hybrid screens is indicated.

(C–G) HEK293 cells were transfected with the constructs indicated on top of each panel. Immunoprecipitations were carried out with HA antibodies that recognize TMIE-HA, followed by western blotting to detect coexpressed proteins. The upper rows show the results of coimmunoprecipitation (CoIP) experiments; following immunoprecipitation, the proteins were resolved on gels and subsequently detected by western blotting with the antibodies indicated on the right. The lower rows (Input) are controls and show protein concentration in the extracts prior to immunoprecipitation; protein extracts were loaded directly onto gels and then analyzed with the antibodies indicated on the right to ensure that the extracts in different experiments contained similar amounts of input protein.

(H) Model for interactions of TMIE with LHFPL5 and different PCDH15 isoforms.

mechanotransduction channels in hair cells. LHFPL5, a tetraspan protein that is linked to inherited forms of deafness (Longo-Guess et al., 2005; Shabbir et al., 2006), binds to PCDH15 and is localized to the tip-link region (Xiong et al., 2012). *Lhfpl5* mutations affect tip-link assembly and the conductance and adaptation properties of the transducer channel, suggesting that LHFPL5 is closely associated with the channel. Structurally and functionally, LHFPL5 resembles auxiliary subunits of other ion channels such as the TARP subunits of AMPA receptors (Jackson and Nicoll, 2011; Straub and Tomita, 2012), suggesting that LHFPL5 like TARPs is an allosteric regulator of transducer channel function (Xiong et al., 2012).

To identify additional critical components of the mechanotransduction complex of hair cells, we have carried out yeast two-hybrid screens with newly generated cochlear libraries. Here we report that PCDH15 and LHFPL5 bind to TMIE, a protein with two transmembrane domains that has previously been linked to inherited forms of deafness (Mitchem et al., 2002; Naz et al., 2002). We demonstrate that TMIE is an evolutionary conserved protein that is essential for mechanotransduction by hair cells. We also show that TMIE establishes a critical link between the PCDH15/LHFPL5 complex and the pore-forming subunits of the transduction channel. Significantly, mutations in TMIE that have been linked to inherited forms of deafness in humans perturb its interaction with tip links and affect transduction, suggesting that the disease is caused by defects in the mechanotransduction machinery of hair cells. Our findings identify TMIE as an essential component of the mechanotransduction machinery of hair cells, provide insights into its mechanisms of action, and reveal an unanticipated complexity in the composition of the mechanotransduction machinery of hair cells that has important implications for the regulation of channel activity in different hair cells and along the tonotopic axis of the cochlea.

## RESULTS

### TMIE Binds to PCDH15 and LHFPL5

In order to identify proteins that are constituents of the mechanotransduction machinery of hair cells, we thought to identify proteins that interact with PCDH15 and/or LHFPL5 at the lower end of tip links. We purified RNA from the organ of Corti and generated three yeast two-hybrid libraries, one for soluble proteins, one for type I transmembrane proteins, and one for type II transmembrane proteins. We then carried out yeast two-hybrid screens with a fragment of PCDH15 encompassing the two membrane-proximal cadherin repeats, the transmembrane domain and the cytoplasmic domain (Figure 1B). Alternative splicing generates different PCDH15 isoforms named CD1, CD2, and CD3 that differ in their cytoplasmic domains (Figure 1B). We used for our experiments the PCDH15-CD2 isoform, since we had determined that this isoform is sufficient to rescue mechanotransduction in hair cells lacking other PCDH15 isoforms (data not shown). We also screened our yeast two-hybrid libraries with full-length LHFPL5 (Figure 1B). Remarkably, we identified TMIE, a protein with two transmembrane domains (Figure 1B) that has previously been linked to deafness (Mitchem et al., 2002; Naz et al., 2002), as a putative interaction partner for both LHFPL5 and PCDH15 (data not shown).

To verify that TMIE interacts with PCDH15 and LHFPL5, we carried out pull-down experiments with extracts from HEK293 cells that were transfected to express an HA-tagged version of TMIE together with PCDH15 or LHFPL5. TMIE interacted with PCDH15-CD2, but only weakly, with its close homologs PCDH15-CD1 and PCDH15-CD3 or with control CDH2-GFP (Figures 1C and 1D). Occasionally, TMIE protein was resolved on gels into two bands (Figure 1C), which could represent differentially glycosylated forms. Alternatively, a fraction of TMIE may be cleaved into two fragments (Gleason et al., 2009). Interactions between PCDH15-CD2 and TMIE were disrupted when the cytoplasmic domain encoded by the CD2-specific exon was deleted from the PCDH15-CD2 full-length construct (Figure 1E). TMIE also interacted with LHFPL5 in pull-down assays (Figure 1F).

We have previously shown that interactions between LHFPL5 and PCDH15 are mediated by the transmembrane domain of PCDH15 as well as by a short membrane-proximal fragment of PCDH15 on the cytoplasmic site that is common between PCDH15-CD1, -CD2, and -CD3 isoforms (Figure 1B) (Xiong et al., 2012). We therefore wondered whether LHFPL5 might facilitate interactions of TMIE even with PCDH15-CD1 and PCDH15-CD3 isoforms by formation of a ternary complex. We coexpressed TMIE together with LHFPL5 and each of the three PCDH15 isoforms in HEK293 cells. Remarkably, in the presence of LHFPL5, antibodies against TMIE-HA coprecipitated PCDH15-CD1, -CD2, and -CD3; LHFPL5 was present in all three protein complexes (Figure 1G; data not shown). We conclude that TMIE and LHFPL5 form a ternary complex with each of the three PCDH15 isoforms. TMIE binds to PCDH15-CD2 directly and via LHFPL5, but interactions between TMIE and PCDH15-CD1 and -CD3 depend on LHFPL5. Thus, the geometry of the PCDH15/LHFPL5/TMIE complex differs in the presence of distinct PCHD15 isoforms (Figure 1H).

### TMIE Function and Expression in Hair Cells

Previous studies have shown that mice with a point mutation in *Tmie* that leads to a truncation of its C terminus are deaf (Mitchem et al., 2002). To confirm and extend these findings, we generated mice with a predicted *Tmie*-null mutation caused by an in-frame insertion of a *LacZ* transgene into the *Tmie* gene ($Tmie^{LacZ}$ mice) (Figure 2A). A second mouse line was generated that carries a floxed *Tmie* allele ($Tmie^{flox}$) (Figure 2A). $Tmie^{LacZ/LacZ}$ mice were deaf as determined by measuring the auditory brainstem response (ABR) to broadband click stimuli in 4-week-old animals (Figure 2C). Similarly, mice were deaf when we inactivated TMIE expression throughout inner ear development using *Pax2-Cre* mice (Ohyama and Groves, 2004) (Figures 2B and 2C). Next we crossed $Tmie^{flox/flox}$ mice with *prestin-CreER*$^{T2}$ mice, which carry a tamoxifen-inducible Cre transgene that is specifically expressed in outer hair cells (OHCs) (Fang et al., 2012). We then induced recombination at P8 and P10 by injection of 4-hydroxytamoxifen and analyzed hearing function 3 weeks later. The mutant mice were deaf, indicating that the function of OHCs was affected (Figures 2B and 2C). We then studied the phenotype of mice obtained by crossings of $Tmie^{flox/flox}$ mice with *Pax2-Cre* and *prestin-CreER*$^{T2}$ mice in more detail. Measurements of responses to pure tones revealed that the mutant offspring obtained with both Cre mouse lines were deaf across the entire analyzed frequency spectrum (Figure 2D). Distortion product otoacoustic emissions (DPOAEs) were nearly eliminated (Figures 2E and 2F). It was somewhat surprising that ABRs and pure tone ABRs were so severely affected following inactivation of *Tmie* in OHCs only using *prestin-Cre* since inner hair cell (IHC) function should be preserved. However, it has previously been reported that the organ of Corti degenerates in *Tmie*-deficient mice by 3 weeks of age (Chung et al., 2007). Thus, inactivation of *Tmie* in OHCs might lead to degenerative changes that affect not only OHCs, but also the overall structure of the organ of Corti including IHCs.

To further define the cell types in the inner ear that express *Tmie*, we took advantage of the LacZ transgene in $Tmie^{LacZ}$ mice. We stained histological sections of $Tmie^{LacZ/+}$ mice with X-Gal and observed that LacZ expression was confined to IHCs and OHCs (Figure 3A). To define the subcellular localization of TMIE in hair cells, we stained cochlear whole mounts at P4 with an antibody to TMIE. The antibody detected TMIE expression in the stereocilia of IHCs and OHCs (Figure 3B). Imaging of IHCs at higher resolution revealed expression near the tips of the shorter rows of stereocilia, but not or only weakly near the tips of the longest stereocilia (Figure 3B, upper right), which is consistent with a localization in the region of the lower insertion site of tip links. No signal was observed in $Tmie^{LacZ/LacZ}$ mice (Figure 3B, lower right), confirming the specificity of the signal. Unfortunately, our antibodies were not of sufficient quality for immunogold localization studies. However, to independently confirm the immunolocalization data, we took advantage of our recently described gene-transfer method for hair cells that we now term injectoporation because it combines plasmid microinjection with electroporation (Figure 3C) (Xiong et al., 2012, 2014). Using injectoporation, we express a cDNA encoding a TMIE-HA fusion protein in hair cells at P4 and analyze expression of the transgene 2 days later. TMIE-HA accumulated at the tips of the

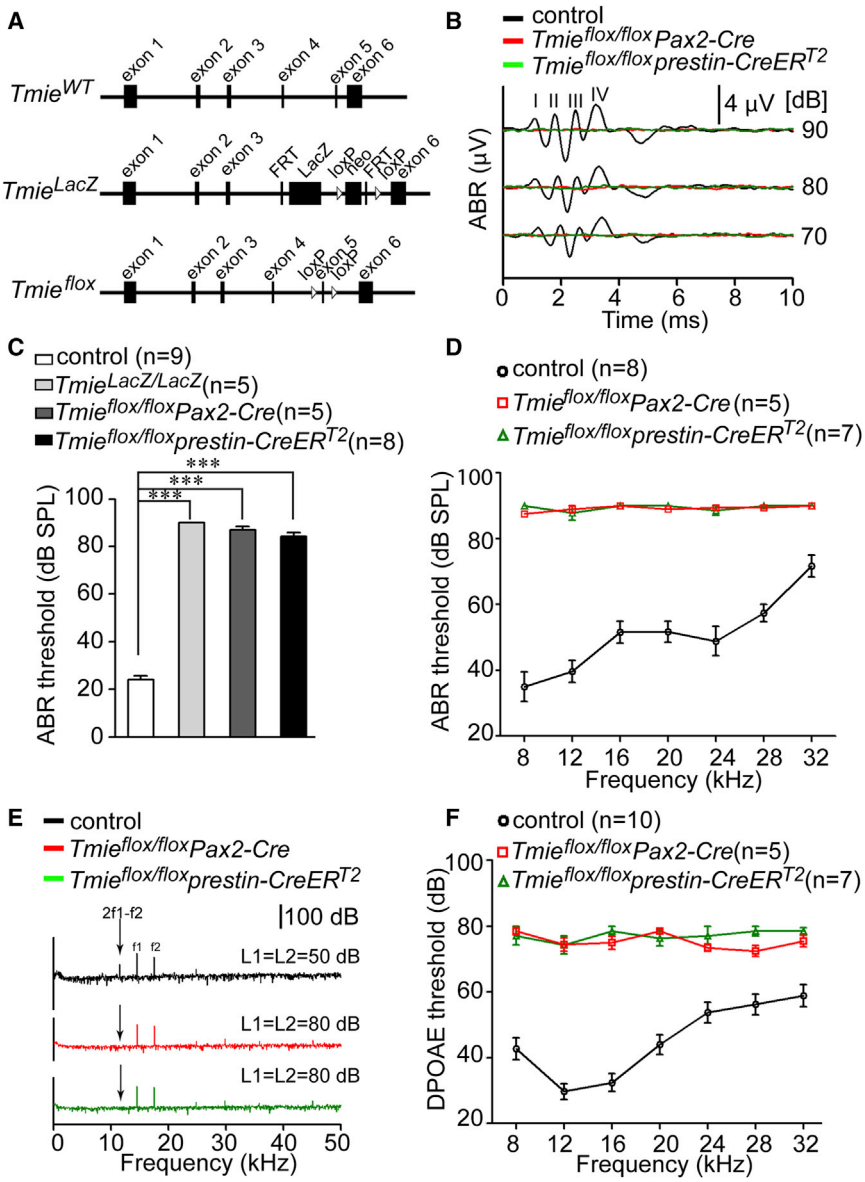


**Figure 2. Analysis of Hearing Function in *Tmie*-Deficient Mice**

(A) Diagram of the various *Tmie* alleles used in the current study.

(B) Representative ABR traces to click stimuli in the indicated control and mutant mice at 4 weeks of age.

(C) Statistic results of ABR thresholds to click stimuli at 4 weeks of age.

(D) ABR thresholds to pure tones at 4 weeks of age.

(E) Representative DPOAE response spectra from wild-type and mutant mice at a single stimulus condition (median primary frequency, 16 kHz; f1, 14.5 kHz; f2, 17.4 kHz; 2f1–f2, 11.6 kHz). Note the 2f1–f2 peak (black arrow), which is absent in mutant mice.

(F) DPOAE thresholds at different frequencies in animals at 4 weeks of age. In (C), (D), and (F) the number of analyzed mice is indicated in brackets. All values are mean ± SEM. ***$p < 0.001$, by Student's t test in (C) and two-way ANOVA in (D) and (F).

shorter rows of stereocilia (Figure 3C), providing additional evidence that TMIE is localized near the lower end of tip links. This localization pattern is consistent with the finding that PCDH15 and LHFPL5, which bind to TMIE, are also localized in this domain of stereocilia (Ahmed et al., 2006; Kazmierczak et al., 2007; Xiong et al., 2012). Thus, we conclude that TMIE is localized in stereocilia at least in part near the lower tip-link insertion site. So far, we have not observed any differences in expression levels of TMIE along the length of the cochlear duct, but additional studies will be necessary to address this point more conclusively.

## Analysis of Mechanotransduction Currents in *Tmie*-Deficient Hair Cells

The localization of TMIE in hair cells and its interaction with PCDH15 and LHFPL5 prompted us to determine the extent to which TMIE is necessary for mechanotransduction by hair cells. Transducer currents were measured at a holding potential of −70 mV. Hair bundles from P5 to P8 OHCs in *Tmie*$^{LacZ/LacZ}$ mice, which were well preserved (Figure 5), were stimulated with a stiff glass probe that was controlled by a piezoelectric actuator. In control wild-type mice, excitatory stimuli elicited transducer currents that reached at maximal deflection peak currents of 420.8 ± 26.9 pA (Figures 4A and 4B). In control *Lhfpl5* mutant mice, transducer currents were reduced to approximately 10% of normal as previously reported (Figures 4G–4I) (Xiong et al., 2012). Strikingly, no transducer currents could be evoked in OHCs from *Tmie*$^{LacZ/LacZ}$ mice (Figures 4A and 4B). Similar observations were also made in IHCs (Figures 4C and 4D). Initial recordings were conducted in a solution containing 1.5 mM $Ca^{2+}$. It has been reported that a reduction in the extracellular $Ca^{2+}$ concentration leads to an increase in channel conductance at rest (Crawford et al., 1991; Kimitsuki and Ohmori, 1992). We therefore recorded transducer currents in OHCs in 0.02 mM $Ca^{2+}$, but still could not elicit transducer currents in *Tmie*-deficient hair cells (Figures 4E and 4F). We conclude that TMIE is essential for normal mechanotransduction by IHCs and OHCs.

## Hair Bundle Morphology and Tip Links in *Tmie*$^{LacZ/LacZ}$ Mice

Defects in the morphology of hair bundles or in tip-link integrity could cause the mechanotransduction defects in *Tmie*-deficient mice. We therefore analyzed hair bundles from *Tmie*$^{LacZ/LacZ}$ mice by scanning electron microscopy at P7 (Figure 5A), an age

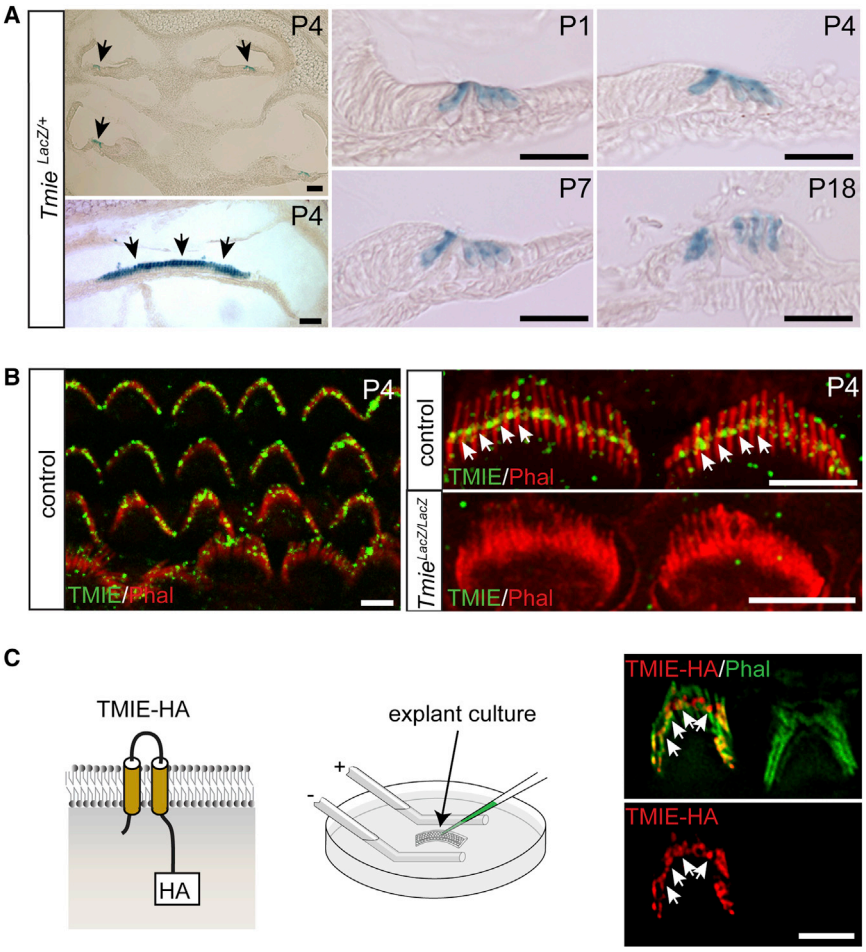


**Figure 3. Expression of TMIE in Hair Cells**

(A) Sections of the inner ear of *Tmie*$^{LacZ/+}$ mice at the indicated ages were stained for LacZ. Note expression of *Tmie* in hair cells in the cochlea (upper left panel, arrows; panels in the middle and on the right) and vestibule (lower left panel, arrows).

(B) Cochlear whole mounts from C57BL/6 mice at P4 were stained for TMIE (green) and phalloidin (red). Left: note the localization of TMIE in stereocilia of IHCs and OHCs. Right: higher-magnification view of IHCs showing TMIE immunoreactivity near the tip link region; no staining was observed in *Tmie*$^{LacZ/LacZ}$ mice.

(C) Cochlear explants were prepared at P4 and injectoporated to express TMIE-HA. After 2 days, the cells were stained with HA antibodies. Note the expression of TMIE-HA in the tip-link region (arrows). Scale bars, (A) 50 μm; (B and C) 3 μm.

that we used for most of our transducer current recordings. Hair bundle morphology was minimally affected in *Tmie*$^{LacZ/LacZ}$ mice. No obvious defects were observed in IHCs, but bundles of OHCs were somewhat abnormal and seemed to assume more of a U shape than the typical V shape. However, rows of stereocilia of graded heights were observed in IHCs and OHCs, and they were linked into a tight bundle without obvious splaying or length variations in stereocilia (Figure 5A). The defects in morphology are unlikely to cause the complete loss of transduction, which is consistent with our previous findings that revealed that transducer currents can be evoked in hair bundles showing substantially greater disruptions in morphology than observed in *Tmie*-deficient mice (Xiong et al., 2012).

Next, we quantified tip-link numbers following our previously described procedures (Xiong et al., 2012). There was no statistically significant difference in the number of tip links in IHCs and OHCs between wild-type and *Tmie*$^{LacZ/LacZ}$ mice (Figures 5B and 5C). We therefore conclude that the mechanotransduction defects in *Tmie*$^{LacZ/LacZ}$ mice are not primarily caused by abnormal hair bundle development or defects in tip-link assembly.

## Analysis of Interactions between TMIE and TMC1/2

Previous studies have shown mechanotransduction currents can no longer be evoked when hair bundles of hair cells lacking TMC1 and TMC2 are deflected in the direction of their longest stereocilia (Kim et al., 2013). We therefore wondered whether TMIE might cooperate with TMC proteins in the regulation of mechanotransduction. We coexpressed TMIE-HA (Figure 3D) together with either TMC1 or TMC2 in HEK293 cells and analyzed interaction by coimmunoprecipitation experiments. For immunoprecipitation and detection we introduced a Myc tag at the N terminus of TMC1 and TMC2, since previous studies have shown that available antibodies to TMC1/2 are of limited quality. An epitope tag at the N terminus of these proteins does not appear to interfere with protein function (Kawashima et al., 2011). We consistently observed that it was significantly more difficult to express TMC2 in HEK293 cells when compared to TMC1 (Figure 5D). However, neither TMC1 nor TMC2 interacted detectably with TMIE, at least when expressed in HEK293 cells (Figure 5D). Similarly, when we carried immunolocalization experiments in transfected HEK293 cells, we observed that TMIE was not colocalized with either TMC1 or TMC2. While TMIE was localized to the cell membrane, TMC1 and TMC2 remained within vesicles inside the cell (Figure 5E).

Finally, we wanted to determine whether TMIE might regulate the distribution of TMC proteins in hair cells. Previous studies have shown that TMC1/2 cannot be detected in hair cells with available antibodies. However, an epitope-tagged TMC2 construct was localized to stereocilia (Kawashima et al., 2011). We therefore expressed Myc-TMC2 by injectoporation in hair cells. Myc-TMC2 was targeted to stereocilia of OHCs in both wild-type and *Tmie*$^{LacZ/LacZ}$ mice (Figure 5F). We conclude that effects in the transport of TMC2 (and probably TMC1) into stereocilia probably do not explain the mechanotransduction defect in OHCs from *Tmie*-deficient mice. However, further studies will be necessary to analyze the functional relationship between TMIE and TMC1/2.

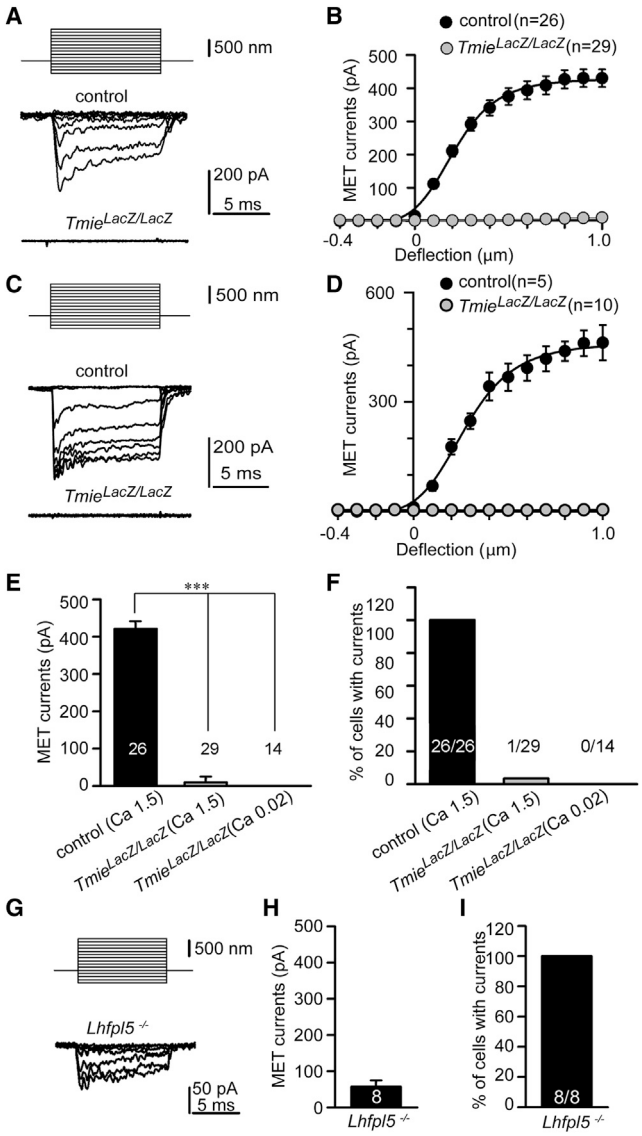


**Figure 4. Mechanotransduction Currents in *Tmie*-Deficient Hair Cells**

(A and C) Examples of transduction currents in OHCs (A) and IHCs (C) from wild-type and *Tmie*$^{LacZ/LacZ}$ mice at P7 in response to a set of 10 ms hair bundle deflections ranging from −400 nm to 1,000 nm (100 nm steps) at a holding potential of −70 mV.

(B and D) Current displacement plots obtained from similar data as shown in (A) and (C). Data in (B) are for OHCs and in (D) for IHCs.

(E) Peak transduction currents in OHCs from control and *Tmie*$^{LacZ/LacZ}$ mice at P5–P8.

(F) Number of OHCs with current.

(G) Examples of transduction currents in OHCs from *Lhfpl5*$^{-/-}$ mice at P7 in response to a set of 10 ms hair bundle deflections ranging from −400 nm to 1,000 nm (100 nm steps).

(H) Peak mechanotransduction currents in OHCs from control and *Lhfpl5*$^{-/-}$ mice at P7.

(I) Number of OHCs with current. In (B), (D), (E), (F), (H), and (I) the number of analyzed hair cells is indicated in brackets. All values are mean ± SEM. ***p < 0.001, by Student's t test.

## Reverse-Polarity Currents in OHCs from *Tmie*$^{LacZ/LacZ}$ Mice

We wondered whether TMIE might be a pore-forming subunit of the mechanotransduction channel. We therefore expressed in HEK293 cells TMIE protein either alone or together in various combinations with LHFPL5, TMC1, TMC2, and/or PCDH15. We were not able to elicit mechanically activated currents with any combination of proteins (data not shown). As a control, we expressed the Piezo1 channel in HEK293 cells and observed robust Piezo1-dependent mechanically evoked currents as previously reported (data not shown) (Coste et al., 2010).

Reverse-polarity stimulation of *Tmc1*/*Tmc2* double-deficient hair bundles leads to the robust activation of a mechanotransduction current, raising the possibility that pore-forming subunits of the transduction channel are still present in *Tmc1*/*Tmc2*-deficient hair cells, but that their location might be changed (Kim and Fettiplace, 2013; Smalla et al., 2000). Consistent with this model, similar reverse-polarity currents are also observed after disruption of tip links (Alagramam et al., 2011; Kim et al., 2013; Marcotti et al., 2014). We wondered if a similar reverse-polarity current is detectable in *Tmie*-deficient hair cells. We therefore established the fluid-jet stimulation system in our laboratory that has previously been used to deflect hair bundles both in the normal and reverse-polarity direction (Kim et al., 2013). We could evoke regular normal-polarity currents in wild-type hair cells (Figure 6A). Robust reverse-polarity currents were observed in hair cells following the disruption of tip links and in hair cells from *Tmc1*/*Tmc2* double-mutant mice (Figures 6A and 6B). In addition, we observed similar reverse-polarity currents in *Tmie*-deficient hair cells (Figures 6A and 6B), raising the possibility that pore-forming subunits of the mechanotransduction are still present in *Tmie*-deficient hair cells.

## Rescue of Mechanotransduction in *Tmie*$^{LacZ/LacZ}$ Mice

To further define the mechanisms by which TMIE affects mechanotransduction in hair cells, we analyze possible functional interactions with TMC1/2 and LHFPL5. We have recently shown that injectoporation is useful to express the genetically encoded $Ca^{2+}$ sensor G-CaMP3 (Tian et al., 2009) in hair cells and to then analyze mechanotransduction by changes in the fluorescence intensity of G-CaMP3 (Xiong et al., 2012, 2014). Following stimulation, fluorescence intensity increased robustly in OHCs of wild-type mice expressing G-CaMP3 (Figures 6C and 6D). Little increase was observed upon stimulation of OHCs from *Tmie*-deficient mice (Figures 6C and 6D). However, mechanotransduction was restored to similar levels as in wild-type mice by expression of TMIE (Figures 6C and 6D), providing further evidence that defects in mechanotransduction in *Tmie*-deficient hair cells are an acute phenomenon, and are not caused by developmental hair cell defects.

Next, we analyzed the extent to which mechanotransduction in *Tmie*-deficient hair cells can be rescued by overexpression of its interaction partner LHFPL5 or by coexpression of both TMC1 and TMC2. We coinjectoporated G-CaMP3 with expression vectors encoding full-length cDNAs for LHFPL5 or TMC1 together with TMC2 in *Tmie*-deficient hair cells. No rescue of transduction was observed (Figure 6E). Similarly, when we expressed G-CaMP3 and TMIE in hair cells from *Lhfpl5*$^{-/-}$ mice

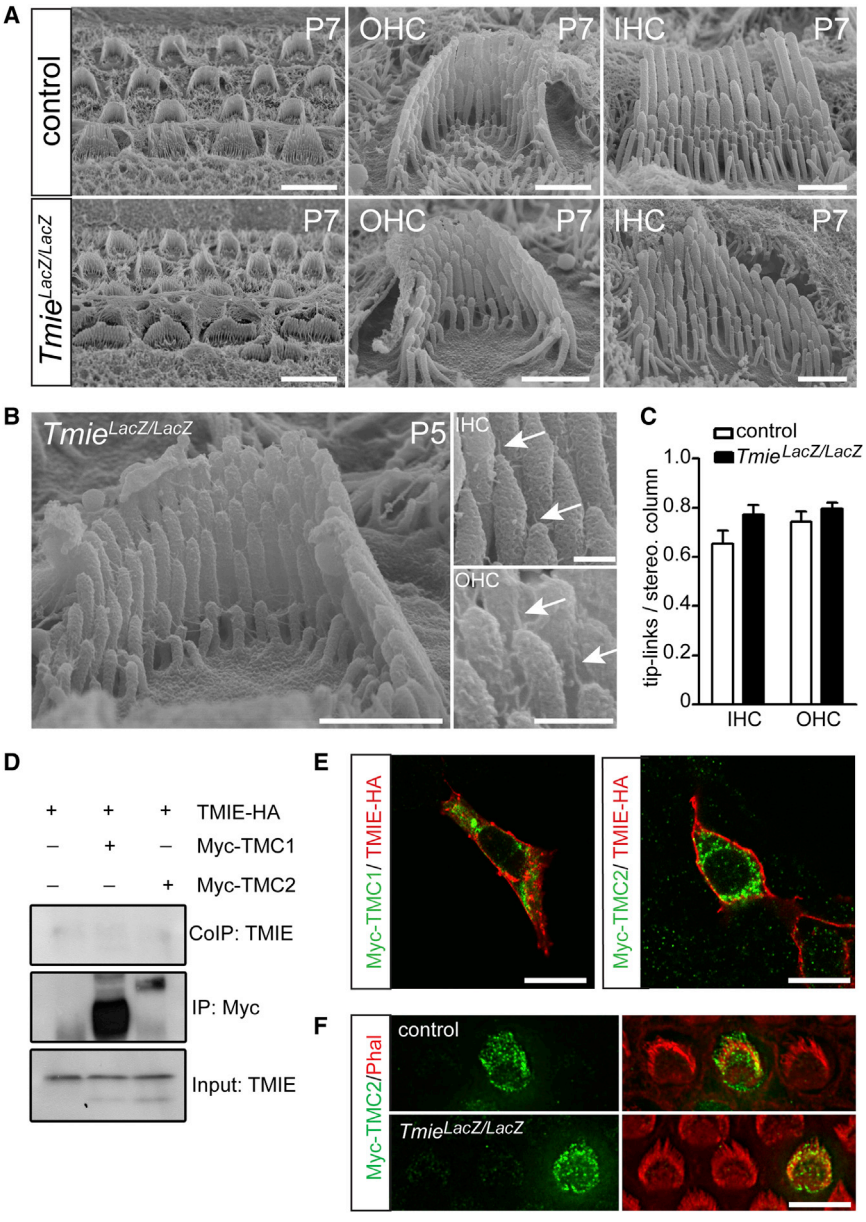


**Figure 5. Hair Bundle Morphology, Tip Links, and Lack of Interactions with TMC1/2**

(A) Scanning electron microscopy analysis of hair bundles from wild-type and *Tmie*$^{LacZ/LacZ}$ mice in the midapical cochlea at P7.

(B) High-resolution images showing tip links (arrows) in OHCs and IHCs.

(C) Quantification of tip-link numbers at P7.

(D) HEK293 cells were transfected with the constructs indicated on top of each panel. Immunoprecipitations were carried out with Myc antibodies that recognize Myc-TMC1 or Myc-TMC2, followed by western blotting to detect TMIE-HA. The lowest row shows input protein; the upper rows show CoIP and IP results.

(E) HEK293 cells were transfected to express Myc-TMC1, Myc-TMC2, and TMIE-HA. Cells were stained 2 days later to detect TMC2 and TMIE. Note that TMIE is at the cell surface and TMC1/2 in vesicles within the cell with little overlap between the two proteins.

(F) OHCs from wild-type C57BL/6 mice and *Tmie*$^{LacZ/LacZ}$ mice were injectoporated at P4 to express Myc-TMC2. Cells were stained 2 days later for Myc-TMC2 (green) and with phalloidin (red). Note that Myc-TMC2 is localized to stereocilia in wild-type and mutant animals. Scale bars, (A) left panels 5 μm; middle and right panels 1 μm; (B) left panel 1 μm; right panels 0.25 μm; (E and F) 4 μm.

(Xiong et al., 2012), we could not rescue their transduction defects (Figure 6F). We thus conclude that neither LHFPL5 nor TMC1 or TMC2 can substitute for the essential function of TMIE in mechanotransduction.

## Functional Analysis of *Tmie* Mutations Linked to Hearing Loss in Humans

We reasoned that we might obtain insights into the function of TMIE by studying more subtle *Tmie* mutations. Three recessive mutations in *Tmie* have been described that cause hearing loss in humans (Naz et al., 2002). The three mutations lead to changes of single amino acids in the C-terminal cytoplasmic domain of TMIE (Figure 7A). The murine and human TMIE proteins are highly homologous, and the amino acids that are affected by the mutations in the human gene are conserved throughout evolution (Figure 7B). We therefore introduced the deafness-causing mutations into the cDNA encoding murine TMIE and expressed the proteins by transfection in HEK293 cells. Two of the mutant proteins, TMIE-R82C and TMIE-R85W, showed a similar membrane localization pattern as the wild-type protein, but the TMIE-R93W protein was no longer transported to the cell surface of HEK293 cells (Figure 7C). We then expressed the three proteins by injectoporation in mechanosensory hair cells. TMIE-R82C and TMIE-R85W were still targeted to stereocilia, but no such targeting was observed for TMIE-R93W (Figure 7D). Next we analyzed the effect of TMIE mutations on interactions with PCDH15-CD2 using pull-down assays. Strikingly, all three mutations drastically affected interactions of TMIE with PCDH15-CD2, while a random mutation that has not been associated with disease (K138R) had no effect on interactions between TMIE and PCDH15-CD2 (Figure 7E).

We next determined the extent to which mutations in *TMIE* that are linked to deafness can rescue transduction defects in *Tmie*-deficient hair cells. We therefore expressed by injectoporation wild-type TMIE and TMIE proteins carrying either the R85W or R93W mutations in hair cells from *Tmie*$^{LacZ/LacZ}$ mice. Transducer currents were measured at a holding potential of −70 mV. Wild-type TMIE effectively rescued transduction. The

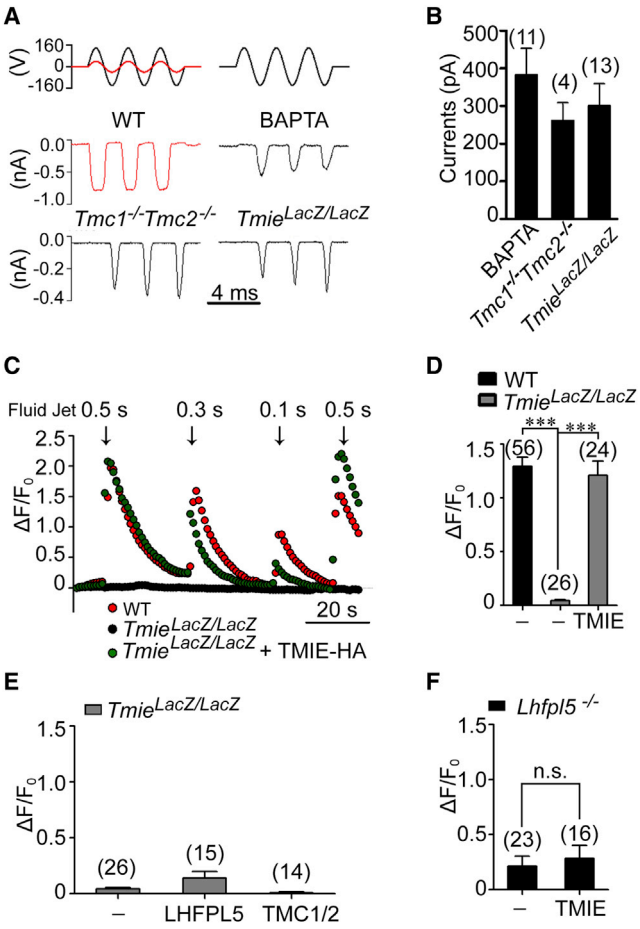


**Figure 6. Reverse-Polarity Currents and Evaluation of Functional Interactions of TMIE with TMC1/2 and LHFPL5**

(A) Examples of mechanotransduction currents in response to sinusoidal deflection of hair bundles at P5 for wild-type C57BL/6 mouse with and without BAPTA treatment, for *Tmc1*/*Tmc2* double-knockouts (Kim et al., 2013), and for *Tmie*$^{LacZ/LacZ}$ mutant mice. All recordings were from apical OHCs at a holding potential of −70 mV; stimulus monitor, the driving voltage to the fluid jet, is shown at the top. A positive driving voltage denotes displacement toward the tallest edge of the hair bundle. Note that the response after BAPTA treatment, in *Tmc1*/*Tmc2* double-knockout and in *Tmie*$^{LacZ/LacZ}$-mutant mice, occurs on the opposite phase of the stimulus to those in the controls.

(B) Quantitative analysis of similar data as shown in (A).

(C) Representative example demonstrating fluid-jet induced $Ca^{2+}$ response in G-CaMP3-expressing OHCs from controls, *Tmie*$^{LacZ/LacZ}$ mutants, and *Tmie*$^{LacZ/LacZ}$ mutants following re-expression of TMIE. OHCs were transfected at P4 and cultured for 2 days in vitro. Sequential fluid-jet pulse durations were 0.1 s, 0.3 s, and 0.5 s. For quantitative analysis (D–F), the amplitude of the second $Ca^{2+}$ response peak was measured.

(D) Quantification of similar $Ca^{2+}$ responses as shown in (C).

(E) OHCs from *Tmie*$^{LacZ/LacZ}$ mutants were injectoporated to express G-CaMP3 and LHFPL5, or G-CaMP3 and both TMC1 and TMC2. Changes in fluorescence intensity following fluid-jet stimulation of hair bundles were recorded 2 days later.

(F) OHCs from *Lhfpl5*$^{-/-}$ mutants were injectoporated to express TMIE. Changes in fluorescence intensity following fluid-jet stimulation of hair bundles were recorded two days later. In (B), (D), (E), and (F) the number of analyzed hair cells is indicated. All values are mean ± SEM. ***$p < 0.001$, by Student's t test. n.s., not significant.

R93W mutation was completely ineffective in rescuing transduction, while small currents could be observed following the expression of R85W (Figure 7F). Taken together, these data suggest that the three mutations in the cytoplasmic domain of TMIE are part of a protein domain that mediates interactions of TMIE with the tip link. The TMIE-R93W mutation affects in addition cell surface transport of TMIE, suggesting that defects in protein transport and in interactions with tip links are causally linked to the mechanotransduction defects caused by mutations in *Tmie*.

## Perturbation of Interactions between TMIE and PCDH15-CD2 Affect Transduction

To provide further evidence that TMIE mediates interactions with the tip link that are important for transduction, we wanted to devise a strategy that perturbs the binding of TMIE to PCDH15. Previous studies have shown that overexpression of protein domains that mediate specific interactions between molecules can disrupt functional interactions, thus acting as dominant-negative (dn) proteins. For example, overexpression of the cytoplasmic domain of cadherin proteins without their extracellular domain can disrupt cadherin signaling (Kintner, 1992). We reasoned that overexpression of the C-terminal protein domains that mediate interactions between PCDH15-CD2 and TMIE might also disrupt the protein complex and therefore affect transduction (Figures 8A and 8B). We therefore generated several C-terminal fragments to identify one that is still properly targeted to stereocilia. This was achieved by expressing a construct consisting of part of the extracellular domain, the second transmembrane domain, and the C-terminal cytoplasmic domain (Figures 8A and 8C). We will refer to this construct as dnTMIE. In HEK293 cells, overexpression of dnTMIE affected interactions between TMIE and PCDH15-CD2 (Figures 8D and 8F). Significantly, dnTMIE also perturbed interactions with LHFPL5 (Figures 8E and 8F), thus providing a useful tool to investigate the extent to which the ternary complex between TMIE, LHFPL5, and PCDH15 is critical for transduction. Notably, when we expressed dnTMIE together with G-CaMP3 in mechanosensory hair cells, the mechanosensory response caused by hair bundle deflection was dramatically reduced (Figure 8G). No such inhibition was observed when we expressed control full-length TMIE in hair cells (Figure 8G), or dnTMIE carrying the three point mutations that have been linked to hearing loss in humans (Figures 8A and 8H). Furthermore, overexpression of a protein fragment encompassing the cytoplasmic domain of PCDH15 that is specific to the PCDH15-CD2 isoform drastically reduced interactions of TMIE with PCDH15-CD2 and transduction (Figures 8A and 8I–8K). We conclude that the C-terminal domain of TMIE mediates interactions with PCDH15 and LHFPL5 that are likely critical for force coupling between the tip link and the transduction channel (Figure 8L). The functional importance of the C-terminal region of TMIE is reinforced by genetic evidence in mice and humans; deletion of the C terminus in *spinner* mice (Mitchem et al., 2002) and point mutations in the C terminus in humans (Naz et al., 2002) cause deafness.

## DISCUSSION

We reveal here an unanticipated complexity in the mechanotransduction machine of cochlear hair cells and demonstrate

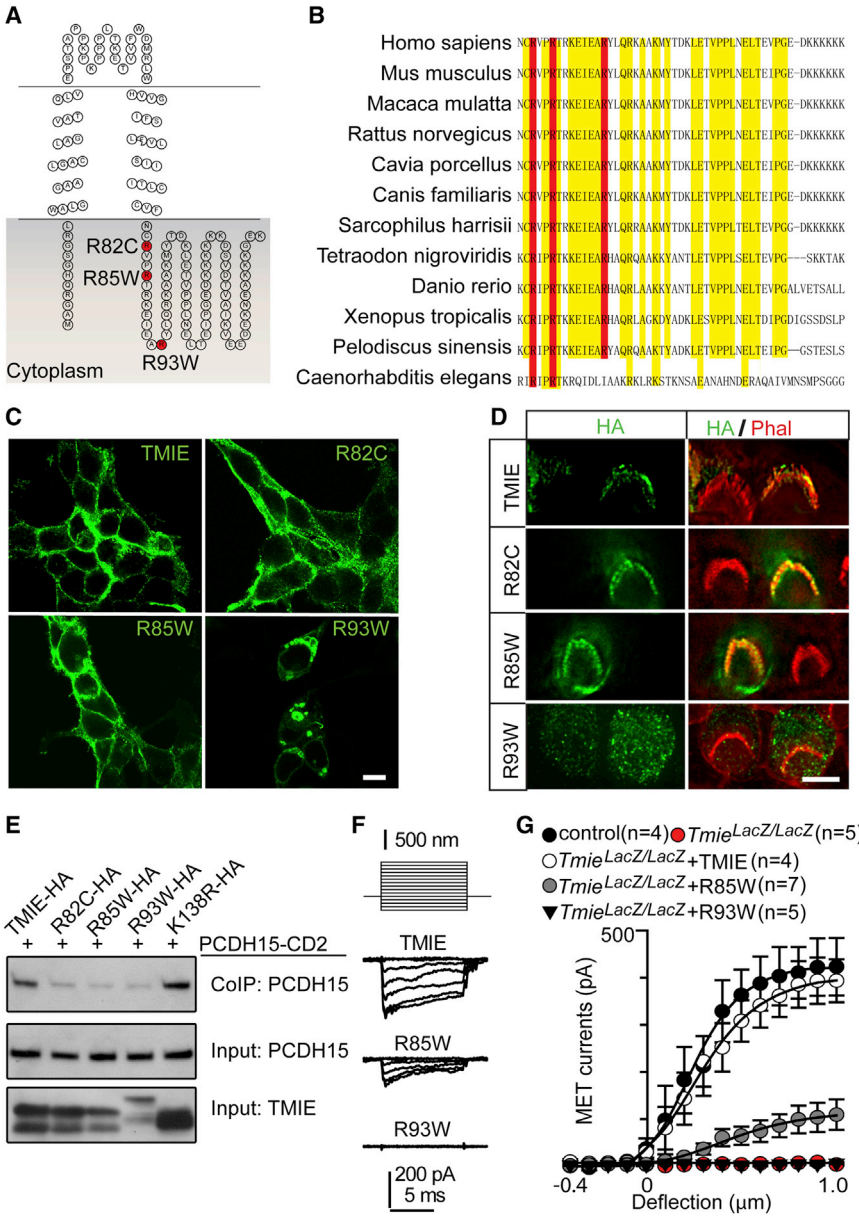


**Figure 7. Analysis of TMIE Proteins with Mutations Linked to Deafness**

(A) Diagram of TMIE indicating three point mutations in the cytoplasmic domain.

(B) Sequence alignment of the part of the cytoplasmic domain of TMIE that contains the mutations linked to deafness. Conserved amino acids are highlighted in yellow; the amino acids that are mutated are in red.

(C) HEK293 cells were transfected to express wild-type TMIE or the indicated mutant forms. Note that TMIE, TMIE-R82C, and TMIE-R85W localized to the cell membrane, whereas TMIE-R93W remained within the cytoplasm.

(D) OHCs were injectoporated at P4 to express the indicated HA-tagged TMIE constructs. Cells were stained 2 days later for the expression of HA-TMIE (green) and phalloidin (red). Note that PCDH15-R93W was no longer localized to stereocilia.

(E) HEK293 cells were transfected with the constructs indicated on top of each panel. Immunoprecipitations were carried out with HA antibodies that recognize wild-type and mutant TMIE, followed by western blotting to detect coexpressed PCDH15-CD2. The lower rows show input protein; the upper rows show CoIP results.

(F and G) OHCs from *Tmie*$^{LacZ/LacZ}$ mice were injectoporated to express wild-type TMIE-HA or the indicated mutant TMIE proteins. Mechanotransduction was measured 2 days later at a holding potential of −70 mV. In (F) representative recordings from single cells are shown. (G) shows current displacement plots. Values in (G) are mean ± SEM. Scale bar, (C) 10 μm; (D) 4 μm.

that TMIE is one essential component of this molecular machine. In the simplest model of mechanotransduction, one might anticipate that the tip-link protein PCDH15 directly binds to the pore-forming subunits of the transduction channel. In contrast, our data suggest that TMIE forms a critical link between PCDH15 and the transduction channel. Mutations in TMIE that have been linked to inherited forms of deafness in humans disrupt these interactions, suggesting that deafness in the affected patients is a direct consequence of a failure of the transduction machinery of their hair cells. Intriguingly, alternative splicing of the cytoplasmic domain of PCDH15 regulates the mechanisms by which TMIE interacts with PCDH15 (Figures 1H and 8L). This suggests that variations in the specific composition of the tip link might affect channel gating in yet-to-be-defined ways, for example, along the tonotopic axis of the cochlea or between hair cells of the cochlea and vestibule that are activated by mechanical signals of distinct frequencies.

Previous studies have shown that microphonic potentials are abolished in *Tmie*-deficient zebrafish. The mutant fish also show defects in hair bundle morphology and in the integrity of tip links (Gleason et al., 2009), but it has remained unclear whether the phenotype is caused by direct effects on transduction or by indirect effects due to developmental or degenerative defects (Shen et al., 2008). Others have shown that hair cells in mice lacking *Tmie* are no longer permeated by FM1-43 and dihydrostreptomycin, two compounds that are thought to enter hair cells through transduction channels (Park et al., 2013). However, the cause of the phenotype had remained unclear since transduction or tip-link integrity had not been evaluated in the mutant mice. We now demonstrated directly that TMIE is an essential component of the mechanotransduction machinery of hair cells, but that it is not essential for tip-link formation. Instead, TMIE functionally couples PCDH15 and LHFPL5 at tip links to the transduction channel. Loss of tip links in *Tmie*-deficient zebrafish is therefore likely a degenerative phenotype. Consistent with this model, hair bundles in *Tmie*-deficient mice show degenerative changes by P15 (Mitchem et al., 2002).

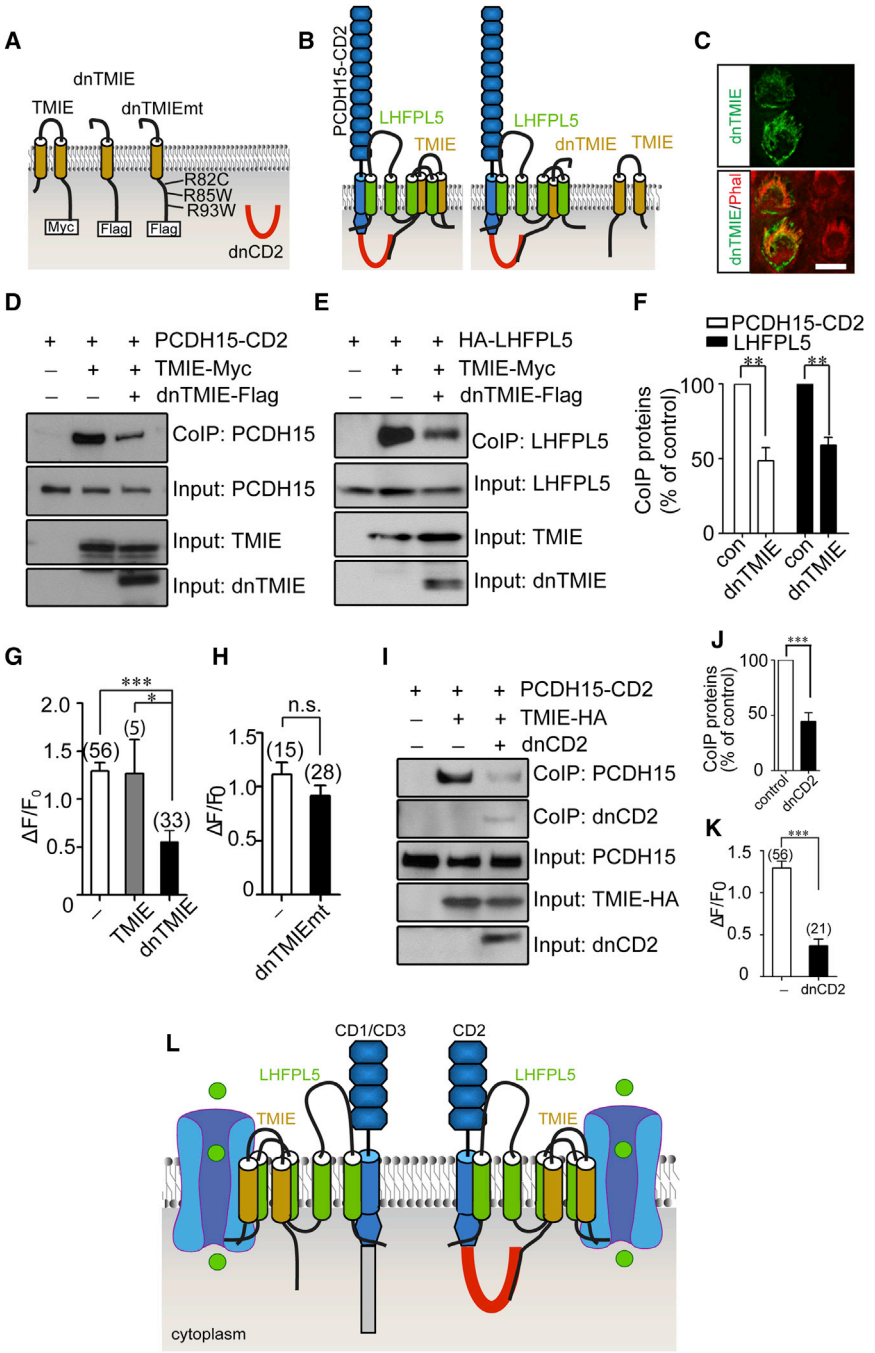


**Figure 8. Perturbations of Interactions between PCDH15-CD2 and TMIE**

(A) Diagram of the constructs used for the experiments.

(B) Rationale for the experiments. Expression of dnTMIE-FLAG is predicted to disrupt interactions of TMIE-Myc with PCDH15-CD2 and HA-LHFPL5, while dnTMIEmt is predicted to have no effect on interactions.

(C) OHCs were injectoporated at P4 to express dnTMIE-HA. Expression of dnTMIE-HA was evaluated 2 days later by immunhistochemistry. Note expression of dnTMIE-HA in hair bundles.

(D and E) HEK293 cells were transfected with the constructs indicated on top of each panel. Immunoprecipitations were carried out with Myc antibodies that recognize TMIE-Myc, followed by western blotting to detect coexpressed proteins. The lower rows show input protein; the upper rows show coimmunoprecipitation (CoIP) results. Note that coexpression of dnTMIE-Myc reduced interactions with PCDH15-CD2 (D) and HA-LHFPL5 (E).

(F) Quantification of dominant-negative effects on protein interaction by scanning of similar gels as shown in (D) and (E). The values are derived by quantifying three independent experiments.

(G and H) Expression of G-CaMP3 alone or together with full-length control TMIE, dnTMIE, or dnTMIEmt in OHCs at P4 and analysis of mechanotransduction 2 days later. dnTMIE, but not dnTMIEmt or TMIE, affected transduction.

(I) HEK293 cells were transfected with the constructs indicated on top of each panel. Immunoprecipitations were carried out with HA antibodies that recognize TMIE-HA, followed by western blotting to detect coexpressed proteins. Note that coexpression of dnCD2 reduced interactions of TMIE with PCDH15-CD2.

(J) Quantification of dominant-negative effects on protein interaction by scanning of similar gels as shown in (I). The values are derived by quantifying three independent experiments.

(K) Expression of G-CaMP3 alone or together with dnCD2 in OHCs at P4 and analysis of mechanotransduction 2 days later. In (G), (H), and (K) the number of analyzed OHCs is indicated. Values are mean ± SEM. ***$p < 0.001$, by Student's t test.

(L) Model of TMIE function in hair cells. In our model, TMIE is critical for force coupling between tip link and channel. TMIE interacts with PCDH15-CD1, -CD2, and -CD3 via LHFPL5, and it also binds directly to PCDH15-CD2. TMC1/2 were omitted from the model, since their relation to the indicated proteins is unclear. Scale bar, (C) 4 μm.

Mechanotransduction currents that are evoked by deflection of the hair bundles in the normal, excitatory direction are abolished in the absence of TMIE, a phenotype that has also been observed for hair cells lacking both TMC1 and TMC2 (Kim and Fettiplace, 2013; Smalla et al., 2000). $Ca^{2+}$ permeability and channel conductance are differentially affected by TMC1 and TMC2 (Kim et al., 2013; Kim and Fettiplace, 2013; Pan et al., 2013). It has therefore been proposed that TMC1 and TMC2 are pore-forming subunits of the transduction channel (Pan et al., 2013). However, when hair bundles of *Tmc1/Tmc2* double-mutant mice are deflected toward the shortest stereocilia, robust transduction currents are observed (Kim and Fettiplace, 2013; Smalla et al., 2000). The reverse- and normal-polarity currents have similar properties suggesting that TMC1 and TMC2 may not be the pore-forming subunits of the transduction channel, but accessory molecules (Kim and Fettiplace, 2013; Smalla et al., 2000). Reverse-polarity transducer currents are also observed when tip links are disrupted (Alagramam

et al., 2011; Kim et al., 2013; Marcotti et al., 2014), suggesting that tip links are essential to localize the channel within stereocilia and to impinge directional sensitivity on channel gating. While it cannot be excluded that the reverse-polarity current requires a channel that is distinct from the tip link-coupled channel, it seems plausible that in the absence of TMC1 and TMC2 the localization of the pore-forming subunits of the normally tip link-coupled transduction channel is altered, thus leading to similar reverse-polarity currents as observed in the absence of tip links (Kim et al., 2013). Since tip links are preserved in *Tmie*-deficient mice, reverse-polarity currents in their hair cells might be explained best by a disruption of the connection between the tip link and the transduction channel. We could not demonstrate either physical or functional interactions between TMIE and TMC1/2, but a recent study suggests that TMC1/2 proteins can interact with PCDH15 (Maeda et al., 2014). Thus, several proteins of the transduction machinery including TMC1/2, LHFPL5, and TMIE can interact with PCDH15, suggesting that the tip link interacts directly with a supramolecular transduction complex. Further biochemical and structural studies will be critical to define the spatial arrangement of the different proteins in the complex. It will also be important to determine the extent to which all these proteins are stably associated at tip links or if some are only transiently present during development or as transport components.

TMIE binds directly to PCDH15-CD2, but only indirectly via LHFPL5 to PCDH15-CD1 and PCDH15-CD3 (Figures 1H and 8L). It therefore appears that alternative splicing of the PCDH15 cytoplasmic domain regulates the specific geometry of the ternary PCDH15, LHFPL5/TMIE protein complexes (Figures 1H and 8L). What could the functional consequences of these differences be, and what is the specific role of LHFPL5, which has previously been shown to regulate the conductance properties of mechanotransduction channels (Xiong et al., 2012)? As one possibility, the distribution of PCDH15 isoforms might vary between cochlear and vestibular hair cells, between OHCs and IHCs, or along the tonotopic axis of the cochlea. In fact, analysis of PCDH15 isoform expression suggests variations in the expression of specific isoforms at least within the developing cochlea (Ahmed et al., 2006). Similarly, LHFPL5 expression levels might vary between different hair cell types and along the cochlea's tonotopic axis. Since mechanotransduction is not grossly altered in mice lacking either PCDH15-CD1, -CD2, or -CD3 (Webb et al., 2011), it appears that several PCDH15 isoforms can function at tip links at least at early postnatal ages. In hair cells of adult mice, the PCDH15-CD2 isoform appears to be essential for transduction (Pepermans et al., 2014), suggesting complex temporal regulatory mechanisms. Notably, the electrophysiological properties of hair cells in mice lacking individual PCDH15 isoforms or LHFPL5 have only been studied in OHCs in the apical cochlea. Based on the findings reported here, it will be interesting to analyze in detail transduction in OHCs and IHCs of PCDH15/LHFPL5-mutant mice at different tonotopic positions, as well as differences in hair cell function between the cochlea and vestibule.

Deafness in the *spinner* mouse line is caused by a mutation that truncates TMIE within the C-terminal cytoplasmic domain (Mitchem et al., 2002). Three point mutations in TMIE that have been linked to recessive forms of deafness in humans (Naz et al., 2002) are also located in the C-terminal cytoplasmic domain of TMIE. These findings suggest that the C-terminal cytoplasmic domain of TMIE that mediates interactions with PCDH15 and LHFPL5 is critical for transduction, indicating that the molecular pathogenesis by which mutation in *Tmie* causes disease can be explained by defects in the transmission of force from tip links onto transduction channels. Notably, hair cell morphology appears normal in *Tmie*-deficient mice at early postnatal ages, which might provide a therapeutic window for the treatment of *Tmie*-related sensorineuronal deafness.

## EXPERIMENTAL PROCEDURES

### Mouse Strains, ABR, and DPOAE Measurement

Strategies for generating knockout mice followed published procedures. In brief, homology arms were amplified from genomic DNA by PCR. To generate $Tmie^{flox}$ mice, a gene-targeting vector was generated that replaced exon 5 with a DNA fragment containing a pGK-neomycin cassette, which was flanked by Flpe sites, and exon 5, which was flanked by LoxP sites. The targeting vector was electroporated into 129P2/OlaHsd embryonic stem cells. Correctly targeted clones were used to generate chimera and crossed to FLP deleter mice to remove the pGK-neomycin selection cassette. To genotype the $Tmie^{flox}$ allele, the following primers were used: 5′-CAGTCCAACTGCAGCCTGC CCTGG-3′ and 5′-CTTTCTAGAGAATAGGAAC TTCGCGGCCGCATAACT-3′. To generate $Tmie^{LacZ}$ mice, constructs were purchased (KOMP) and electroporated into 129P2/OlaHsd embryonic stem cells. For genotyping of the $Tmie^{LacZ}$ mice, the following primers were used: 5′-ACCCCTCCTCTCCTGC CCTTGCTCC-3′ and 5′-GGGGGTACCGCGTCGAGAAGTTCC-3′. The wild-type *Tmie* allele in $Tmie^{flox}$ and $Tmie^{LacZ}$ mice was genotyped using the following primers: 5′-GGCT CGGTATCTACAGCGAAAGGCGGCC-3′ and 5′-TGCCTGGCTCTGACTAGTTTCTGC AC-3′. To induce Cre activity in crosses with *prestin-creER*$^{T2}$ mice, 30 μl 4-hydroxytamoxifen (10 mg/ml in sunflower oil) was intraperitoneally injected into pups at P8 and P10. ABR and DPOAE measurements were carried out as described (Schwander et al., 2007). *Tmc1/Tmc2* knockout mice (CBA.Cg-*Tmc1*$^{dn}$/AjgJ; B6;129S5-*Tmc2*$^{tm1Lex}$/Mmucd (Kim et al., 2013) were a kind gift from Dr. Fettiplace (University of Wisconsin).

### LacZ Staining

Tissue was fixed for 1 hr in PFA and incubated for 2 days at 4°C in 20% sucrose/PBS. Cryosections were prepared, postfixed for 15 min at room temperature (RT) in 1% PFA, 0.2% glutaraldehyde, 0.02% NP40, and 0.01% sodium deoxycholate, and washed three times in PBS containing 0.02% NP40 and 0.01% sodium deoxycholate. Sections were stained overnight in the 1 mg/ml X-Gal staining solution (25 mM potassium ferricyanide, 25 mM potassium ferrocyanide, 2 mM $MgCl_2$, 1 mg/ml X-Gal diluted in PBS) at 37°C. Sections were washed three times for 20 min in PBS and postfixed overnight at 4°C in 4% PFA. Sections were washed in distilled water, dehydrated, and mounted.

### Whole-Mount Staining and Immunocytochemistry

Cochlear whole-mount staining and immunocytochemistry of HEK293 cells were carried out as described (Xiong et al., 2012). Primary antibodies were as follows: α-TMIE (rabbit; Sigma), α-HA (mouse; Cell Signaling Technology), α-Myc (rabbit; Cell Signaling Technology). Additional reagents were as follows: Alexa Fluor 488-phalloidin, Alexa Fluor 594 goat anti-rabbit, Alexa Fluor 488 goat anti-mouse, and Alexa Fluor 647-phalloidin (Invitrogen).

### Scanning Electron Microscopy

Inner ears were dissected in fixative (2.5% glutaraldehyde; 4% formaldehyde; 0.05 mM HEPES buffer [pH 7.2]; 10 mM $CaCl_2$; 5 mM $MgCl_2$; 0.9% NaCl). A hole was poked at the apex of the cochlea, fixative was flushed through the round window, the sample was fixed for 2 hr at RT, and dissected in washing buffer (0.05 mM HEPES buffer [pH 7.2]; 10 mM $CaCl_2$; 5 mM $MgCl_2$; 0.9%

NaCl). The stria vascularis, Reissner's membrane, and tectorial membrane were removed. Samples were dehydrated and processed to critical drying point in an Autosamdri-815A (Tousimis). Cochlea were mounted with carbon tape and coated with iridium (sputter coater EMS150T S; Electron Microscopy Sciences). Samples were imaged with a Hitachi S-4800-II Field Emission Scanning Electron Microscope. Quantification of hair bundle morphology and tip links was carried out as described (Xiong et al., 2012).

### DNA Constructs, Transfections, Immunoprecipitations, and Western Blots

DNA constructs are described in Supplemental Information. Expression of the constructs, immunoprecipitations, and western blots were carried out as described (Senften et al., 2006). Immunoprecipitation experiments were carried out at least three times to verify the reproducibility of the data. The following antibodies were used for the experiments: α-TMIE (rabbit; Sigma), α-HA (mouse; Cell Signaling Technology), α-Myc (rabbit; Cell Signaling Technology), α-FLAG (rabbit; Sigma), α-GFP (Xiong et al., 2012), α-PCDH15 (Kazmierczak et al., 2007), α-LHFPL5 (Longo-Guess et al., 2005).

### Injectoporation

The organ of Corti was isolated from P0–P8 mice as described (Grillet et al., 2009). For recording, tissue was transferred to the recording chamber and fixed to a nylon mesh. For culture, the organ of Corti was cut into three pieces, which were placed in DMEM/F12 medium with 1.5 μg/ml ampicillin. For electroporation, glass electrodes (2 μm diameter) were used to deliver plasmid (1 μg/μl in 1× HBSS) to the sensory epithelium. A series of three pulses was applied at 1 s intervals with a magnitude of 60 V and duration of 15 ms (ECM 830 Square Wave Electroporator; BTX). For $Ca^{2+}$ imaging, we used G-CaMP3 (Addgene 22692). Hair cells were imaged on an upright Olympus BX51WI microscope mounted with a 60× water-immersion objective and Qimaging ROLERA-QX camera, controlled by MicroManager 1.3 software (Edelstein et al., 2010). Hair bundles were stimulated with a fluid jet applied through a glass electrode (2-μm-tip diameter) filled with bath solution. Stimuli were applied using Patchmaster 2.35 software (HEKA) and 20 psi air pressure. Images were collected with a 2 s sampling rate. A series of fluid-jet stimulations (0.1, 0.3, 0.5 s) was applied (60 s intervals). Responses induced by 0.3 s fluid-jet stimulation were used for quantitative analysis.

### Electrophysiology

Recordings were carried out in the midapical region of the cochlea. During recording, a Peri-Star Peristaltic Pump (WPI) was used to perfuse artificial perilymph (in mM): 144 NaCl, 0.7 $NaH_2PO_4$, 5.8 KCl, 1.3 $CaCl_2$, 0.9 $MgCl_2$, 5.6 glucose, and 10 H-HEPES (pH 7.4). In some recordings, $Ca^{2+}$ concentration was reduced to 0.02 mM. To record reverse-polarity currents in OHCs from wild-type animals, 5 mM BAPTA was added to the bath solution. Borosilicate glass with filament (Sutter) was pulled with a P-97 pipette puller (Sutter), and polished with MF-830 microforge (Narishige) to resistances of 3–5 MΩ. Hair bundles were deflected with a glass pipette mounted on a P-885 piezoelectric stack actuator (Physik Instrumente). The tip of the pipette was fire-polished to ~4 μm diameter to fit the shape of OHC bundles. The actuator was driven with voltage steps that were low-pass-filtered at 10 KHz with a 900CT eight-pole Bessel filter (Frequency Devices). The output driving voltage to the actuator stack was monitored by an oscilloscope to ensure a rise time < 50 μs. The tip of the probe was cleaned in chromic acid to allow adherence to hair bundles. The reverse-polarity currents were elicited from OHCs using a fluid jet from a pipette (tip diameter of 10–15 μm). Sinusoidal force stimulus was applied to a 27-mm-diameter piezoelectric disc to produce fluid jet. The position of the pipette delivering the fluid jet was positioned at the modiolar side of the hair bundles and adjusted to elicit maximal MET currents. The sinusoids (40 Hz) were generated with Patchmaster 2.35 software (HEKA) and filtered at 1.0 kHz with 900CT eight-pole Bessel filter (Frequency Devices). Whole-cell recordings were carried out, and currents were sampled at 100 KHz with an EPC 10 USB patch-clamp amplifier operated by Patchmaster 2.35 software (HEKA). To record macroscopic currents, the patch pipette was filled with intracellular solution (140 mM KCl, 1 mM $MgCl_2$, 0.1 mM EGTA, 2 mM Mg-ATP, 0.3 mM Na-GTP, and 10 mM H-HEPES [pH7.2]). Cells were clamped at −70 mV. The junction potential for the solution in this study was measured to be 4.1 mV and was not corrected.

### Data Analysis

Data analysis was performed using Excel (Microsoft) and Igor Pro 6 (WaveMetrics). Calcium signal (ΔF/F) was calculated with the equation $(F-F_0)/F_0$, where $F_0$ is the averaged fluorescence baseline at the beginning. Transduction current-displacement curves (I(X)) were fitted with a three-state Boltzmann model (Grillet et al., 2009). All data are mean ± SEM. Student's two-tailed unpaired t test was used to determine statistical significance (*$p < 0.05$, **$p < 0.01$, ***$p < 0.001$).

## SUPPLEMENTAL INFORMATION

Supplemental Information includes Supplemental Experimental Procedures and can be found with this article online at http://dx.doi.org/10.1016/j.neuron.2014.10.041.

## ACKNOWLEDGMENTS

We thank Robert Fettiplace and Maryline Beurg for help with establishing the fluid-jet stimulation system, Andy Groves for Pax2-Cre mice, and Jian Zuo for prestin-CreER$^{T2}$ mice. This work was funded with support from the NIH (UM DC005965, DC007704), the Dorris Neuroscience Center, the Skaggs Institute for Chemical Biology, and the Bundy Foundation (UM).

Accepted: October 15, 2014
Published: November 20, 2014

## REFERENCES

Adato, A., Michel, V., Kikkawa, Y., Reiners, J., Alagramam, K.N., Weil, D., Yonekawa, H., Wolfrum, U., El-Amraoui, A., and Petit, C. (2005). Interactions in the network of Usher syndrome type 1 proteins. Hum. Mol. Genet. *14*, 347–356.

Ahmed, Z.M., Goodyear, R., Riazuddin, S., Lagziel, A., Legan, P.K., Behra, M., Burgess, S.M., Lilley, K.S., Wilcox, E.R., Riazuddin, S., et al. (2006). The tip-link antigen, a protein associated with the transduction complex of sensory hair cells, is protocadherin-15. J. Neurosci. *26*, 7022–7034.

Alagramam, K.N., Goodyear, R.J., Geng, R., Furness, D.N., van Aken, A.F., Marcotti, W., Kros, C.J., and Richardson, G.P. (2011). Mutations in protocadherin 15 and cadherin 23 affect tip links and mechanotransduction in mammalian sensory hair cells. PLoS ONE *6*, e19183.

Assad, J.A., Shepherd, G.M., and Corey, D.P. (1991). Tip-link integrity and mechanical transduction in vertebrate hair cells. Neuron *7*, 985–994.

Bahloul, A., Michel, V., Hardelin, J.P., Nouaille, S., Hoos, S., Houdusse, A., England, P., and Petit, C. (2010). Cadherin-23, myosin VIIa and harmonin, encoded by Usher syndrome type I genes, form a ternary complex and interact with membrane phospholipids. Hum. Mol. Genet. *19*, 3557–3565.

Beurg, M., Fettiplace, R., Nam, J.H., and Ricci, A.J. (2009). Localization of inner hair cell mechanotransducer channels using high-speed calcium imaging. Nat. Neurosci. *12*, 553–558.

Boëda, B., El-Amraoui, A., Bahloul, A., Goodyear, R., Daviet, L., Blanchard, S., Perfettini, I., Fath, K.R., Shorte, S., Reiners, J., et al. (2002). Myosin VIIa, harmonin and cadherin 23, three Usher I gene products that cooperate to shape the sensory hair cell bundle. EMBO J. *21*, 6689–6699.

Caberlotto, E., Michel, V., Foucher, I., Bahloul, A., Goodyear, R.J., Pepermans, E., Michalski, N., Perfettini, I., Alegria-Prévot, O., Chardenoux, S., et al. (2011). Usher type 1G protein sans is a critical component of the tip-link complex, a structure controlling actin polymerization in stereocilia. Proc. Natl. Acad. Sci. USA *108*, 5825–5830.

Chung, W.H., Kim, K.R., Cho, Y.S., Cho, D.Y., Woo, J.H., Ryoo, Z.Y., Cho, K.I., and Hong, S.H. (2007). Cochlear pathology of the circling mouse: a new mouse model of DFNB6. Acta Otolaryngol. *127*, 244–251.

Coste, B., Mathur, J., Schmidt, M., Earley, T.J., Ranade, S., Petrus, M.J., Dubin, A.E., and Patapoutian, A. (2010). Piezo1 and Piezo2 are essential components of distinct mechanically activated cation channels. Science *330*, 55–60.

Crawford, A.C., Evans, M.G., and Fettiplace, R. (1991). The actions of calcium on the mechano-electrical transducer current of turtle hair cells. J. Physiol. *434*, 369–398.

Edelstein, A., Amodaj, N., Hoover, K., Vale, R., and Stuurman, N. (2010). Computer control of microscopes using μManager. Curr. Protoc. Mol. Biol. http://dx.doi.org/10.1002/0471142727.mb1420s92.

Fang, J., Zhang, W.C., Yamashita, T., Gao, J., Zhu, M.S., and Zuo, J. (2012). Outer hair cell-specific prestin-CreERT2 knockin mouse lines. Genesis *50*, 124–131.

Gillespie, P.G., and Müller, U. (2009). Mechanotransduction by hair cells: models, molecules, and mechanisms. Cell *139*, 33–44.

Gleason, M.R., Nagiel, A., Jamet, S., Vologodskaia, M., López-Schier, H., and Hudspeth, A.J. (2009). The transmembrane inner ear (Tmie) protein is essential for normal hearing and balance in the zebrafish. Proc. Natl. Acad. Sci. USA *106*, 21347–21352.

Grati, M., and Kachar, B. (2011). Myosin VIIa and sans localization at stereocilia upper tip-link density implicates these Usher syndrome proteins in mechanotransduction. Proc. Natl. Acad. Sci. USA *108*, 11476–11481.

Grillet, N., Xiong, W., Reynolds, A., Kazmierczak, P., Sato, T., Lillo, C., Dumont, R.A., Hintermann, E., Sczaniecka, A., Schwander, M., et al. (2009). Harmonin mutations cause mechanotransduction defects in cochlear hair cells. Neuron *62*, 375–387.

Jackson, A.C., and Nicoll, R.A. (2011). The expanding social network of ionotropic glutamate receptors: TARPs and other transmembrane auxiliary subunits. Neuron *70*, 178–199.

Kawashima, Y., Géléoc, G.S., Kurima, K., Labay, V., Lelli, A., Asai, Y., Makishima, T., Wu, D.K., Della Santina, C.C., Holt, J.R., and Griffith, A.J. (2011). Mechanotransduction in mouse inner ear hair cells requires transmembrane channel-like genes. J. Clin. Invest. *121*, 4796–4809.

Kazmierczak, P., Sakaguchi, H., Tokita, J., Wilson-Kubalek, E.M., Milligan, R.A., Müller, U., and Kachar, B. (2007). Cadherin 23 and protocadherin 15 interact to form tip-link filaments in sensory hair cells. Nature *449*, 87–91.

Kim, K.X., and Fettiplace, R. (2013). Developmental changes in the cochlear hair cell mechanotransducer channel and their regulation by transmembrane channel-like proteins. J. Gen. Physiol. *141*, 141–148.

Kim, K.X., Beurg, M., Hackney, C.M., Furness, D.N., Mahendrasingam, S., and Fettiplace, R. (2013). The role of transmembrane channel-like proteins in the operation of hair cell mechanotransducer channels. J. Gen. Physiol. *142*, 493–505.

Kimitsuki, T., and Ohmori, H. (1992). The effect of caged calcium release on the adaptation of the transduction current in chick hair cells. J. Physiol. *458*, 27–40.

Kintner, C. (1992). Regulation of embryonic cell adhesion by the cadherin cytoplasmic domain. Cell *69*, 225–236.

Kros, C.J., Marcotti, W., van Netten, S.M., Self, T.J., Libby, R.T., Brown, S.D., Richardson, G.P., and Steel, K.P. (2002). Reduced climbing and increased slipping adaptation in cochlear hair cells of mice with Myo7a mutations. Nat. Neurosci. *5*, 41–47.

Kurima, K., Peters, L.M., Yang, Y., Riazuddin, S., Ahmed, Z.M., Naz, S., Arnaud, D., Drury, S., Mo, J., Makishima, T., et al. (2002). Dominant and recessive deafness caused by mutations of a novel gene, TMC1, required for cochlear hair-cell function. Nat. Genet. *30*, 277–284.

Longo-Guess, C.M., Gagnon, L.H., Cook, S.A., Wu, J., Zheng, Q.Y., and Johnson, K.R. (2005). A missense mutation in the previously undescribed gene Tmhs underlies deafness in hurry-scurry (hscy) mice. Proc. Natl. Acad. Sci. USA *102*, 7894–7899.

Marcotti, W., Corns, L.F., Desmonds, T., Kirkwood, N.K., Richardson, G.P., and Kros, C.J. (2014). Transduction without tip links in cochlear hair cells is mediated by ion channels with permeation properties distinct from those of the mechano-electrical transducer channel. J. Neurosci. *34*, 5505–5514.

Marzban, H., Khanzada, U., Shabir, S., Hawkes, R., Langnaese, K., Smalla, K.H., Bockers, T.M., Gundelfinger, E.D., Gordon-Weeks, P.R., and Beesley, P.W. (2003). Expression of the immunoglobulin superfamily neuroplastin adhesion molecules in adult and developing mouse cerebellum and their localisation to parasagittal stripes. J. Comp. Neurol. *462*, 286–301.

Michalski, N., Michel, V., Caberlotto, E., Lefèvre, G.M., van Aken, A.F., Tinevez, J.Y., Bizard, E., Houbron, C., Weil, D., Hardelin, J.P., et al. (2009). Harmonin-b, an actin-binding scaffold protein, is involved in the adaptation of mechanoelectrical transduction by sensory hair cells. Pflugers Arch. *459*, 115–130.

Mitchem, K.L., Hibbard, E., Beyer, L.A., Bosom, K., Dootz, G.A., Dolan, D.F., Johnson, K.R., Raphael, Y., and Kohrman, D.C. (2002). Mutation of the novel gene Tmie results in sensory cell defects in the inner ear of spinner, a mouse model of human hearing loss DFNB6. Hum. Mol. Genet. *11*, 1887–1898.

Maeda, R., Kindt, K.S., Mo, W., Morgan, C.P., Erickson, T., Zhao, H., Clemens-Grisham, R., Garr-Gillespie, P.G., and Nicolson, T. (2014). Tip-link protein protocadherin 15 interacts with transmembrane channel-like protein TMC1 and TMC2. Proc. Natl. Acad. Sci. USA *111*, 12907–12912.

Naz, S., Giguere, C.M., Kohrman, D.C., Mitchem, K.L., Riazuddin, S., Morell, R.J., Ramesh, A., Srisailpathy, S., Deshmukh, D., Riazuddin, S., et al. (2002). Mutations in a novel gene, TMIE, are associated with hearing loss linked to the DFNB6 locus. Am. J. Hum. Genet. *71*, 632–636.

Ohyama, T., and Groves, A.K. (2004). Generation of Pax2-Cre mice by modification of a Pax2 bacterial artificial chromosome. Genesis *38*, 195–199.

Pan, B., Géléoc, G.S., Asai, Y., Horwitz, G.C., Kurima, K., Ishikawa, K., Kawashima, Y., Griffith, A.J., and Holt, J.R. (2013). TMC1 and TMC2 are components of the mechanotransduction channel in hair cells of the mammalian inner ear. Neuron *79*, 504–515.

Park, S., Lee, J.H., Cho, H.J., Lee, K.Y., Kim, M.O., Yun, B.W., and Ryoo, Z. (2013). tmie is required for gentamicin uptake by the hair cells of mice. Comp. Med. *63*, 136–142.

Pepermans, E., Michel, V., Goodyear, R., Bonnet, C., Abdi, S., Dupont, T., Gherbi, S., Holder, M., Makrelouf, M., Hardelin, J.P., et al. (2014). The CD2 isoform of protocadherin-15 is an essential component of the tip-link complex in mature auditory hair cells. EMBO Mol. Med. *6*, 984–992.

Pickles, J.O., Rouse, G.W., and von Perger, M. (1991). Morphological correlates of mechanotransduction in acousticolateral hair cells. Scanning Microsc. *5*, 1115–1124.

Richardson, G.P., de Monvel, J.B., and Petit, C. (2011). How the genetics of deafness illuminates auditory physiology. Annu. Rev. Physiol. *73*, 311–334.

Schwander, M., Sczaniecka, A., Grillet, N., Bailey, J.S., Avenarius, M., Najmabadi, H., Steffy, B.M., Federe, G.C., Lagler, E.A., Banan, R., et al. (2007). A forward genetics screen in mice identifies recessive deafness traits and reveals that pejvakin is essential for outer hair cell function. J. Neurosci. *27*, 2163–2175.

Schwander, M., Kachar, B., and Müller, U. (2010). Review series: The cell biology of hearing. J. Cell Biol. *190*, 9–20.

Senften, M., Schwander, M., Kazmierczak, P., Lillo, C., Shin, J.B., Hasson, T., Géléoc, G.S., Gillespie, P.G., Williams, D., Holt, J.R., and Müller, U. (2006). Physical and functional interaction between protocadherin 15 and myosin VIIa in mechanosensory hair cells. J. Neurosci. *26*, 2060–2071.

Shabbir, M.I., Ahmed, Z.M., Khan, S.Y., Riazuddin, S., Waryah, A.M., Khan, S.N., Camps, R.D., Ghosh, M., Kabra, M., Belyantseva, I.A., et al. (2006). Mutations of human TMHS cause recessively inherited non-syndromic hearing loss. J. Med. Genet. *43*, 634–640.

Shen, Y.C., Jeyabalan, A.K., Wu, K.L., Hunker, K.L., Kohrman, D.C., Thompson, D.L., Liu, D., and Barald, K.F. (2008). The transmembrane inner ear (tmie) gene contributes to vestibular and lateral line development and function in the zebrafish (*Danio rerio*). Dev. Dyn. *237*, 941–952.

Siemens, J., Kazmierczak, P., Reynolds, A., Sticker, M., Littlewood-Evans, A., and Müller, U. (2002). The Usher syndrome proteins cadherin 23 and harmonin

form a complex by means of PDZ-domain interactions. Proc. Natl. Acad. Sci. USA *99*, 14946–14951.

Siemens, J., Lillo, C., Dumont, R.A., Reynolds, A., Williams, D.S., Gillespie, P.G., and Müller, U. (2004). Cadherin 23 is a component of the tip link in hair-cell stereocilia. Nature *428*, 950–955.

Smalla, K.H., Matthies, H., Langnäse, K., Shabir, S., Böckers, T.M., Wyneken, U., Staak, S., Krug, M., Beesley, P.W., and Gundelfinger, E.D. (2000). The synaptic glycoprotein neuroplastin is involved in long-term potentiation at hippocampal CA1 synapses. Proc. Natl. Acad. Sci. USA *97*, 4327–4332.

Söllner, C., Rauch, G.J., Siemens, J., Geisler, R., Schuster, S.C., Müller, U., and Nicolson, T.; Tübingen 2000 Screen Consortium (2004). Mutations in cadherin 23 affect tip links in zebrafish sensory hair cells. Nature *428*, 955–959.

Straub, C., and Tomita, S. (2012). The regulation of glutamate receptor trafficking and function by TARPs and other transmembrane auxiliary subunits. Curr. Opin. Neurobiol. *22*, 488–495.

Tian, L., Hires, S.A., Mao, T., Huber, D., Chiappe, M.E., Chalasani, S.H., Petreanu, L., Akerboom, J., McKinney, S.A., Schreiter, E.R., et al. (2009). Imaging neural activity in worms, flies and mice with improved GCaMP calcium indicators. Nat. Methods *6*, 875–881.

Webb, S.W., Grillet, N., Andrade, L.R., Xiong, W., Swarthout, L., Della Santina, C.C., Kachar, B., and Müller, U. (2011). Regulation of PCDH15 function in mechanosensory hair cells by alternative splicing of the cytoplasmic domain. Development *138*, 1607–1617.

Xiong, W., Grillet, N., Elledge, H.M., Wagner, T.F., Zhao, B., Johnson, K.R., Kazmierczak, P., and Müller, U. (2012). TMHS is an integral component of the mechanotransduction machinery of cochlear hair cells. Cell *151*, 1283–1295.

Xiong, W., Wagner, T., Yan, L., Grillet, N., and Müller, U. (2014). Using injectoporation to deliver genes to mechanosensory hair cells. Nat. Protoc. *9*, 2438–2449.